Applied Catalysis B: Environmental 117–118 (2012) 167–176

Contents lists available at SciVerse ScienceDirect

Applied Catalysis B: Environmental

journal homepage: www.elsevier.com/locate/apcatb

Sulfate storage and stability on representative commercial lean NO_x trap components

Nathan A. Ottinger[1], Todd J. Toops*, Josh A. Pihl, Justin T. Roop, Jae-Soon Choi, William P. Partridge

Fuels, Engines and Emissions Research Center, Oak Ridge National Laboratory, 2360 Cherahala Blvd., Knoxville, TN 37932, USA

ARTICLE INFO

Article history:
Received 2 October 2011
Received in revised form 9 December 2011
Accepted 28 December 2011
Available online 16 January 2012

Keywords:
Sulfur
Lean NO_x trap
DRIFTS
Ceria–zirconia
$MgAl_2O_4$

ABSTRACT

Components found in a commercial lean NO_x trap have been studied in order to determine their impact on sulfate storage and release. A micro-reactor and a diffuse reflectance infrared Fourier transform spectrometer (DRIFTS) were used to compare components $MgAl_2O_4$, $Pt/MgAl_2O_4$, Pt/Al_2O_3, $Pt/Ba/Al_2O_3$, $Pt/CeO_2–ZrO_2$, and $Pt/Ba/CeO_2–ZrO_2$, as well as physical mixtures of $Pt/Al_2O_3 + MgAl_2O_4$ and $Pt/Ba/CeO_2–ZrO_2 + MgAl_2O_4$. Desulfation temperature profiles as well as DRIFTS NO_x and SO_x storage spectra are presented for all components. This systematic approach highlighted the ability of the underlying support to impact sulfate stability, in particular when Ba was supported on ceria–zirconia rather than alumina the desulfation temperature decreased by 60–120 °C. A conceptual model of sulfation progression on the ceria–zirconia support is proposed that explains the high uptake of sulfur and low temperature release when it is employed. It was also determined that the close proximity of platinum is not necessary for much of the sulfation and desulfation chemistry that occurs, as physical mixtures with platinum dispersed on only one phase displayed similar behavior to samples with platinum dispersed on both phases.

1. Introduction

Growing concern about the consequences of global warming and the obvious economic advantages of higher efficiency engines continue to increase interest in lean-burn automobiles. So far, though, their widespread introduction into the marketplace has been limited by the difficulty of meeting emissions restrictions due to ineffective catalytic reduction of tail-pipe NO_x emissions. Though several possible solutions to this problem are being explored, one option that has been extensively studied is the lean NO_x trap (LNT), also known as a NO_x adsorber or NO_x storage reduction (NSR) catalyst. The details of LNT functionality, i.e. cyclical lean/rich operation, dependence on platinum-group metals (PGM), such as Pt, Pd, and Rh, and dependence on alkali/alkaline earth metals, such as Ca, Ba, K, and Na, has been established and well documented [1,2], and thus the details will not be repeated here.

Because of their ability to achieve high NO_x conversions over a range of temperatures without the need for additional on-board reductants such as urea, LNTs are attractive as NO_x reduction catalysts [3,4]. However, in the presence of sulfur, performance is impacted as NO_x storage sites are blocked by sulfur. This impact can alter both performance and selectivity to N_2 or NH_3. How the impact is manifested will depend on the components within the complex LNT catalyst and which one is being affected by sulfur. Using a commercial catalyst, Choi et al. [5–7] have shown that sulfation to 3.4 g S/g_{cat} can reduce NO_x conversion by 40% at 325 and 400 °C as well as increase NH_3 yield at the same temperatures. The authors found that sulfur is stored on Ba, Ce, Mg, and Al phases depending on the dose of sulfur introduced. Additionally, Choi et al. [8,9] have found that desulfation results in a complex desulfation profile which cannot be adequately explained with the present knowledge of LNT sulfur storage and release characteristics. In other studies, Rohr et al. [10] sulfated a $Pt/Pd/Rh/Ba/CeO_2/Al_2O_3$ LNT to 1.3 g S/L_{cat} and found that while Ba was significantly sulfated, Ce and Al_2O_3 did not store sulfur at this level of sulfation. Other studies have shown that sulfur is stored on a variety of LNT components including Ba [5–17], γ-Al_2O_3 [5–24], $MgAl_2O_4$ [24–30], and Ce–Zr mixed oxides [5–7,31–33]. These studies serve to demonstrate that sulfur may be deposited on all of these components found in LNTs, but it is difficult to extract the individual roles of the components in these mixtures.

From this pertinent literature, it was determined that a deeper understanding of the sulfation and desulfation behavior of common LNT components was necessary. This effort aims to improve the understanding of the role of components that exist in this commercial LNT catalyst, a reference catalyst selected by the CLEERS LNT focus group was the emphasis of this study. This catalyst is known to contain Pt, Pd, Rh, Ba, Ce, Zr, Mg, and Al [7], and it was determined that this catalyst fundamentally differs from the typical model

* Corresponding author. Tel.: +1 8659461207; fax: +1 8659461354.
E-mail address: toopstj@ornl.gov (T.J. Toops).
[1] Currently at Cummins Emission Solutions.

0926-3373/$ – see front matter © 2012 Elsevier B.V. All rights reserved.
doi:10.1016/j.apcatb.2011.12.044

Table 1
Component contributions by mass percent.

	Pt	Ba	Al_2O_3	$MgAl_2O_4$	CeO_2–ZrO_2
$MgAl_2O_4$	–	–	–	100	–
$Pt/MgAl_2O_4$	1.0	–	–	99	–
Pt/Al_2O_3	1.5	–	98.5	–	–
$Pt/Ba/Al_2O_3$	0.8	20	79.2	–	–
Pt/CeO_2–ZrO_2	1.0	–	–	–	99
$Pt/Ba/CeO_2$–ZrO_2	0.8	20	–	–	79.2

catalysts being studied in several ways. The first key difference is that the Ba storage phase is almost entirely supported on ceria–zirconia rather than γ-Al_2O_3. This Ba/ceria–zirconia phase also contains a significant amount of Pt/Pd, but not Rh. A second key difference is that there is a significant fraction of $MgAl_2O_4$ in the commercial LNT. This phase generally contains little PGM, but does comprise up to 40 wt% of the washcoat. While there have been some reports as to the potential of $MgAl_2O_4$ in LNT chemistry [24–30] the role here is examined with and without precious metal in direct contact with the material to ascertain the potential of PGM in neighboring oxides to benefit the oxides with low PGM content. Micro-reactor sulfation experiments were employed in order to quantify the affinity of specific LNT components for SO_2 during typical, cyclic operating conditions. After sulfating, the stability of stored SO_2 was probed with desulfation experiments. A diffuse reflectance infrared Fourier transform spectrometer (DRIFTS) was also used to probe the effect that sulfation and mild desulfations have on the NO_x storage and NO_x stability of the LNT components.

2. Experimental

2.1. Components

The components studied fit into two groups: those prepared by wet impregnation and physical mixtures. A full list of the catalysts prepared as well as their formulations is found in Table 1. Physicochemical properties of the studied catalysts including surface area and SO_2 storage capacity are shown in Table 2. T_{20} and T_{90}, the temperatures necessary for 20% and 90% removal of stored sulfur, are also shown in Table 2, and will be used later to describe the stability of sulfur on the studied components.

- $MgAl_2O_4$ (MA) was used directly from the supplier, 99.985% pure from Alfa-Aesar.
- $Pt/MgAl_2O_4$ (PMA) was prepared by the wet impregnation of hydrogen hexachloroplatinate (IV) onto the $MgAl_2O_4$ support described above.
- Pt/Al_2O_3 (PA) was prepared by the wet impregnation of hydrogen hexachloroplatinate (IV) onto commercial grade γ-Al_2O_3 provide by EmeraChem, LLC. The sample was then calcined at 500 °C for 2 h.
- Pt/CeO_2–ZrO_2 (PCZ) was prepared by the wet impregnation of Pt (as $Pt(NH_3)_4(NO_3)_2$) onto CeO_2–ZrO_2 (*Rhodia*, Ce/Zr = 70/30, surface area = 114 m^2/g). The sample was then calcined in air at 550 °C for 2 h.[2]
- $Pt/Ba/Al_2O_3$ (PBA) and $Pt/Ba/CeO_2$–ZrO_2 (PBCZ) were both prepared by the wet impregnation of aqueous barium acetate ($Ba(C_2H_3O_2)_2H_2O$) onto Pt/Al_2O_3 and Pt/CeO_2–ZrO_2, respectively. The samples were then air dried and calcined at 550 °C overnight.
- Physical mixtures of $Pt/Al_2O_3 + MgAl_2O_4$ (PA + MA) and $Pt/Ba/CeO_2$–$ZrO_2 + MgAl_2O_4$ (PBCZ + MA) were created by mixing equal parts by mass of the two catalysts. The PBCZ + MA catalyst is most representative of the commercial catalyst.

2.2. Instrumentation

The micro-reactor used in this study has previously been described in great detail [33,34]. It consists of lean and rich gas banks controlled by a 4-way valve, a bypass line for flow equilibration and calibration, a mass spectrometer (SRS RGA100), and a sulfur analyzer (API Model 100A UV fluorescence SO_2 analyzer). In addition to the main reactor, an oxidation reactor (oxycat) is used to oxidize H_2S to SO_2 because the sulfur analyzer detects only SO_2, and the mass spec is more sensitive to SO_2 than H_2S. The oxycat used was a Pt/Al_2O_3 catalyst coarsely crushed to minimize pressure drop and maintained at 1000 °C in order to prevent SO_2 adsorption. A constant supply of O_2 (7.5 sccm) was fed directly to the oxycat to maintain an oxidizing environment. A similar setup for monitoring SO_2 has been used by Kylhammar et al. [19] and McLaughlin et al. [35], and their protocol was used to account for SO_2 to SO_3 oxidation.

The DRIFTS apparatus has also been previously described [36]. It consists of a MIDAC M2500 spectrometer coupled to a Harrick barrel ellipse diffuse reflectance attachment and an integrated heated stainless steel reaction cell. The reaction cell is capable of achieving sample temperatures of 550 °C and is operated at a pressure of 500 Torr in order to prevent gas stagnation and maintain a seal between the reaction cell and the hemispherical zinc selenide (ZnSe) dome. Mass flow controllers metered the flows of inlet gases. All spectra are presented in absorbance units, and consist of one hundred scans taken at a resolution of 2 cm^{-1}. The background spectra varied for each experiment and are detailed in Section 3. The gases used in DRIFTS experiments were from Air Liquide® and originated from the same cylinders as those used in micro-reactor experiments.

2.3. Characterization

Sulfation and desulfation experiments were performed in a micro-reactor. Samples were ground into a powder, and 75 mg of each catalyst sample was mixed with an equal amount of quartz wool in order to minimize pressure drop across the catalyst bed. In the case of the physical mixtures, 37.5 mg of each catalyst was mixed together and then added to 75 mg quartz wool. The samples were positioned between two plugs of quartz wool in a U tube reactor. Prior to experiments, the catalysts were pretreated for 8 h at 700 °C while cycling 127 s lean and 17 s rich. Lean gases consisted of NO, O_2, CO_2, H_2O, and Ar bal., while rich gases were made up of H_2, CO, CO_2, H_2O, and Ar bal. Specific gas compositions used for pretreatment, sulfation, and desulfation experiments are shown in Table 3.

A total flow rate of 120 sccm (GHSV ~ 30,000 h^{-1}) was used, and SO_2 was introduced at 30 ppm during sulfation experiments. Gas bottles used for experiments were from Air Liquide®, and had the following purities: Ar (99.999%), 10% H_2 (99.999%) in Ar (99.999%), 10% CO (99.97%) in Ar (99.999%), 1% NO (99%) in Ar (99.999%), O_2 (99.9995%), CO_2 (99.997%), and 1000 ppm SO_2 (99.9%) in Ar (99.999%). CO_2, O_2, and H_2O traps removed impurities from Ar lines, and mass flow controllers were used for gas metering.

Three sulfation and desulfation experiments were performed on each catalyst to achieve an equilibrated sulfur state. Sulfation experiments were performed at 400 °C while cycling 127 s lean and 17 s rich. SO_2 was fed at 30 ppm and for long enough to achieve an estimated loading of 5.5 mg S/g_{cat}; actual loading is typically less than this due to sulfur slip. After each sulfation, all weakly bound

[2] Sample prepared by Yaying Ji at the Center for Applied Energy Research in Lexington, Kentucky.

Table 2
Physicochemical properties of components.

Catalyst formulation	Chemical composition	BET surface area (m^2/g)	SO_2 capacity @ ~80 min ($\mu mol/g_{cat}$)	1000 °C TPR SO_2 release ($\mu mol/g_{cat}$)	Percent difference (%)	T_{20} (°C)	T_{90} (°C)
MA	$MgAl_2O_4$	14	112	132	18%	653	816
PMA	$Pt/MgAl_2O_4$	14	193	186	4%	544	789
PA	Pt/Al_2O_3	101	187	174	6%	464	707
PBA	$Pt/Ba/Al_2O_3$	43	199	248	25%	570	855
PA + MA	$Pt/Al_2O_3 + MgAl_2O_4$	–	191	194	2%	480	752
PCZ	$Pt/CeO_2–ZrO_2$	79	204	178	13%	494	570
PBCZ	$Pt/Ba/CeO_2–ZrO_2$	41	195	170	13%	535	797
PBCZ + MA	$Pt/Ba/CeO_2–ZrO_2 + MgAl_2O_4$	–	204	197	3%	531	782

sulfur species were removed by cycling the catalyst at 400 °C for 25 min before desulfating. The inlet gases were then switched to rich conditions, and the catalyst was desulfated. For the first two sulfation experiments, the desulfation was performed from 400 to 700 °C at 10 °C/min. After reaching 700 °C, the temperature was maintained at this level for 1 h. A 400 °C sulfation experiment was performed in between the two 700 °C desulfations. This was followed by a final sulfation and then a desulfation was performed from 400 to 1000 °C at 5 °C/min in order to remove all sulfur species and maximize resolution of sulfur release peaks. As in the 700 °C desulfation, the catalyst was held at 1000 °C for 1 h.

As previously described, a DRIFT attachment in conjunction with a FTIR spectrometer [36] was used to analyze the impact of sulfur on NO storage and stability of the various catalyst components. All DRIFTS experiments were performed with a flow rate of 100 sccm and the gas concentrations are shown in Table 3. The catalysts were first pretreated for 8 h at 350 °C while switching between 0.79% H_2 and 300 ppm NO with 10% O_2 in order to remove all carbonates (all gases used in this study were in an Ar balance). CO and CO_2 were not used in this portion of the study to avoid the formation of convoluting carbonate spectral features. The protocol used for DRIFTS experiments is detailed below and is graphically illustrated in Fig. 1. The same step numbers are used in Fig. 1 to indicate that a given procedure is the same as those which precede it.

1. The catalysts were heated to 500 °C in 5% H_2O to remove any residual NO_x or carbonate surface species before beginning NO_x storage experiments.
2. The catalysts were cooled from 500 to 200 °C, taking background spectra in 5% H_2O every 50 °C. This gives a good background spectrum and allows the removal of gas-phase H_2O from displayed spectra.
3. The NO_x storage behavior was examined; 300 ppm NO, 10% O_2, and 5% H_2O were introduced for 30 min.
4. A temperature programmed desorption to 450 °C was carried out in 5% H_2O.
5. The catalysts were cooled to 200 °C in 5% H_2O and background spectra were taken.
6. A 1 h introduction of 30 ppm SO_2 was performed while cycling 6 min lean and 30 s rich.
   - After sulfating, a 30 min NO_x storage experiment with 300 ppm NO, 10% O_2, and 5% H_2O (step 3b in Fig. 1).
7. The catalysts were then heated to 450 °C in 5% H_2O.
   - Cooled once again to 200 °C and another NO_x storage and TPD experiment were performed (steps 2c–4c in Fig. 1).
8. A TPR was then performed to 500 °C in 0.79% H_2 and 5% H_2O.
   - In the cases of PCZ, PBA, and PBCZ another 30 min NO_x storage experiment was performed (steps 2d and 3d in Fig. 1).

The steps in this sequence were always performed in the same day to minimize baseline shift and improve analysis.

Table 3
Gas compositions used for micro-reactor and DRIFTS switching experiments.

Gas	Micro-Reactor (120 sccm)		DRIFTS (100 sccm)	
	Lean	Rich	Lean	Rich
NO	300 ppm	–	300 ppm	–
O_2	10%	–	10%	–
H_2	–	0.71%	–	0.79%
CO	–	1.19%	–	–
CO_2	5%	5%	–	–
H_2O	5%	5%	5%	5%
SO_2[a]	30 ppm	30 ppm	30 ppm	30 ppm
Ar	Balance	Balance	Balance	Balance

[a] Flowed during sulfation experiments only.

3. Results

3.1. Micro-reactor sulfation and desulfation experiments

Micro-reactor sulfation and desulfation experiments were used to measure the affinity for, and the stability of sulfur on the various LNT components studied. Fig. 2 shows sulfation profiles for the various LNT components. In this figure and hereafter, the components are denoted according to the following abbreviations: $MgAl_2O_4$ (MA), $Pt/MgAl_2O_4$ (PMA), Pt/Al_2O_3 (PA), $Pt/Ba/Al_2O_3$ (PBA), $Pt/Al_2O_3 + MgAl_2O_4$ (PA + MA), $Pt/CeO_2–ZrO_2$ (PCZ), $Pt/Ba/CeO_2–ZrO_2$ (PBCZ), $Pt/Ba/CeO_2–ZrO_2 + MgAl_2O_4$ (PBCZ + MA). As verified with a mass spectrometer attached to the system, the apparent oscillations in Fig. 2 are due to brief sulfur releases during the rich phase. The raw mass spectrum data for amu = 64 in Fig. 3 from a PBA sulfation experiment shows these brief rich phase SO_2 pulses and long lean phase storage troughs. The SO_2 release is dampened and broadened in the SO_2 analyzer because of additional flow, a more tortuous path, and slower response time. The amplitudes of the oscillations in the SO_2 analyzer vary depending on the species, with PBA having the largest oscillation of approximately 4 ppm and the other samples having somewhere in between 4 and 0.1 ppm. This phenomenon will be elaborated on in Section 4.

A typical series of three desulfation experiments is shown in Fig. 4 for the PBA component. The first two profiles shown in Fig. 4a are from desulfations performed to 700 °C at 10 °C/min, whereas the third profile in Fig. 4b is from the final desulfation performed to 1000 °C at 5 °C/min. In all three desulfation experiments, sulfur begins desorbing at 400 °C, and in the two desulfation experiments performed to 700 °C, sulfur continues to come off at a significant level (>5 ppm) for at least 30 min while the catalyst is held at 700 °C. This was typical of all catalysts that had a desulfation temperature higher than 700 °C. Final desulfation experiments performed from 400 to 1000 °C at 5 °C/min are shown for all components in Fig. 5, and the integrated μmol S per gram catalyst released from 400 to 600 °C, 600 to 800 °C, and 800 to 1000 °C is presented in Fig. 6. The results are presented here using the same scale for all samples to

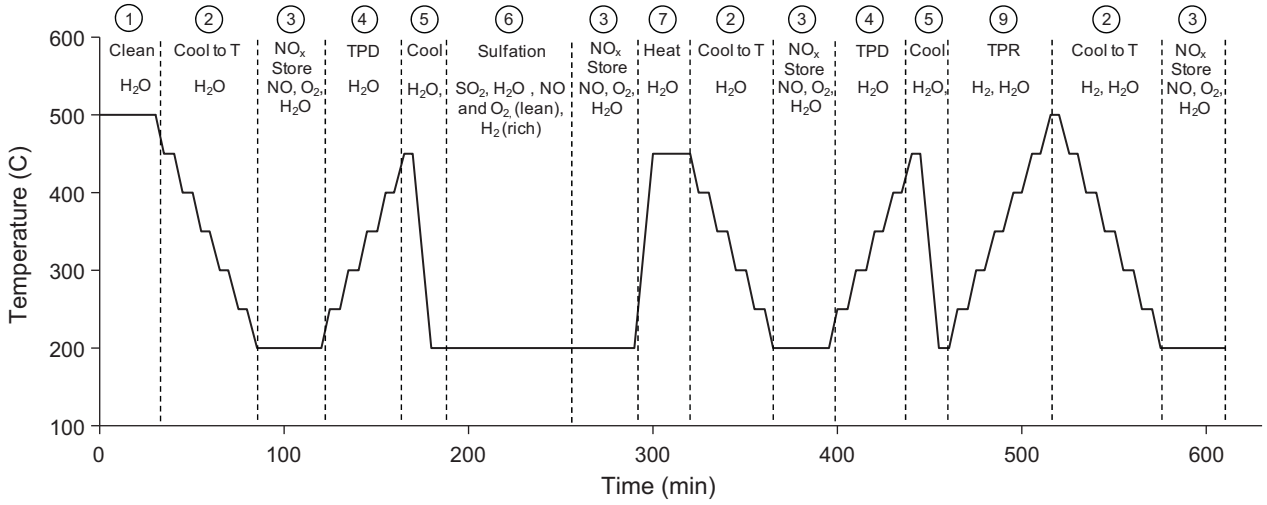

Fig. 1. Protocol for DRIFTS sulfation, desulfation, NO_x storage, and NO_x TPD experiments. Flow rate = 100 sccm.

give a snapshot of each component's behavior for a comparison on an equivalent basis.

3.2. DRIFTS NO_x storage and sulfation experiments

DRIFTS experiments were performed in order to further characterize the stability of stored nitrate and sulfate species as well as evaluate the ability of mild desulfations to restore NO_x capacity. The components studied with DRIFTS included MA, PMA, PA, PBA, PCZ, and PBCZ. Pre-sulfation NO_x storage DRIFTS spectra for the components are all shown in Fig. 7 and their associated

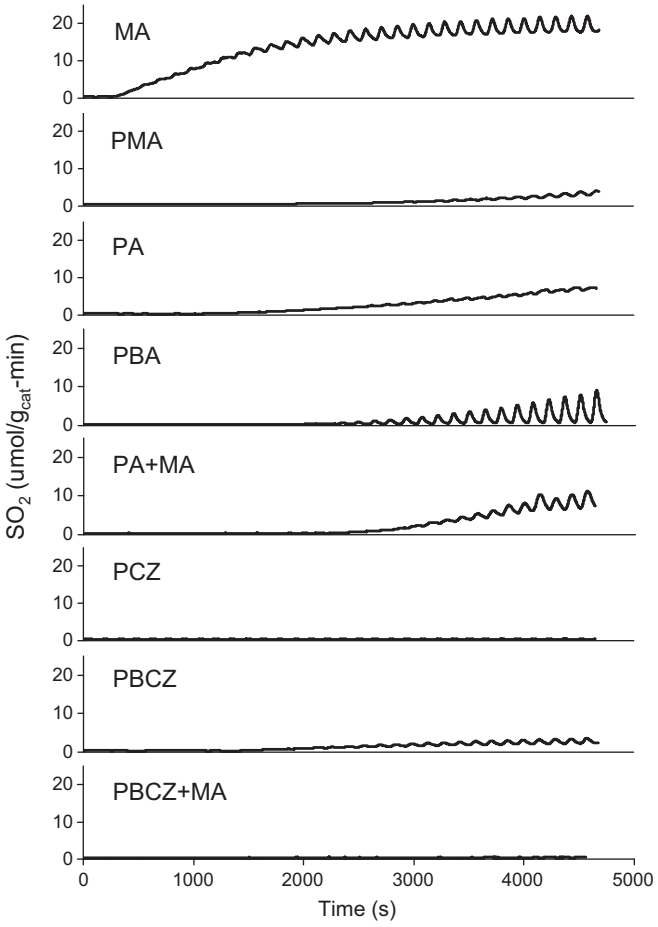

Fig. 2. Cyclic sulfation experiments for all components (lean: 300 ppm NO, 10% O_2; rich: 1.19% CO, 0.71% H_2; both: 30 ppm SO_2 5% CO_2, 5% H_2O, Ar bal.). GHSV ~ 30,000 h^{-1}.

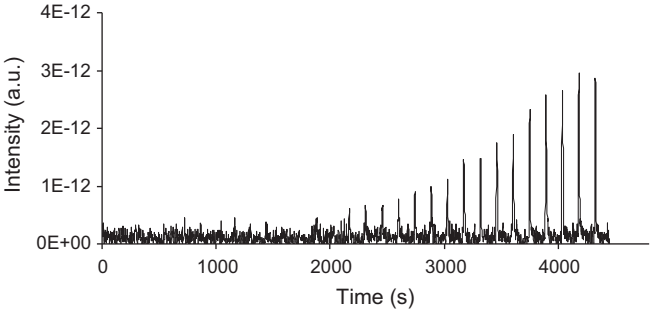

Fig. 3. Raw mass spectrum data (amu = 64) from PBA sulfation experiment shows large rich-cycle sulfur releases.

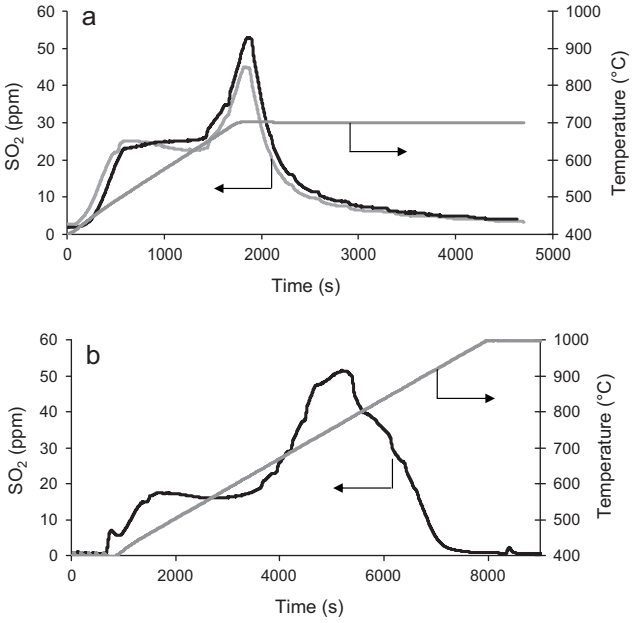

Fig. 4. Desulfation experiments for PBA (a) from 400 to 700 °C at 10 °C/min and (b) 400–1000 °C at 5 °C/min (1.19% CO, 0.71% H_2, 5% CO_2, 5% H_2O, Ar bal.). GHSV ~ 30,000 h^{-1}.

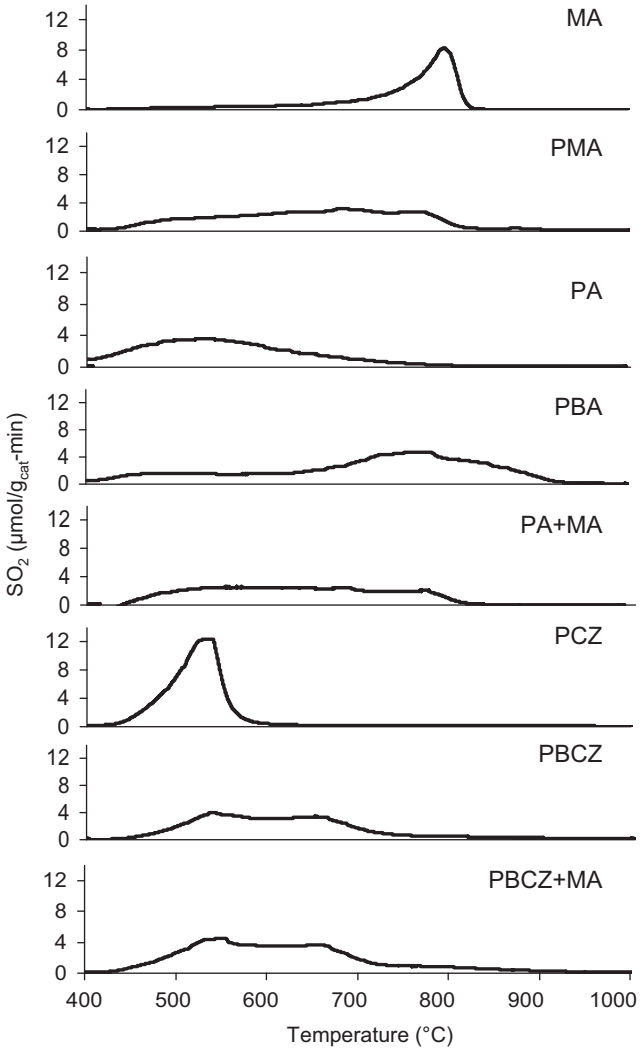

Fig. 5. Final desulfation profile for all components (1.19% CO, 0.71% H_2, 5% CO_2, 5% H_2O, Ar bal.). GHSV ~ 30,000 h^{-1}. Ramp rate: 5 °C/min.

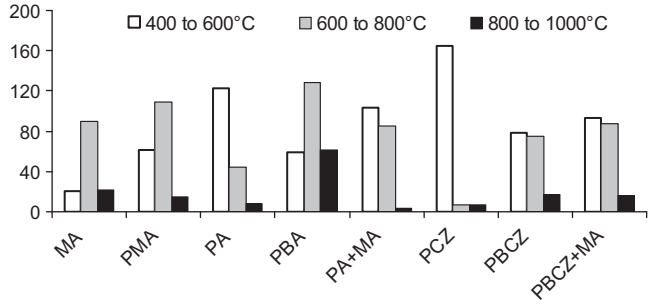

Fig. 6. Sulfur released in μmol S/g_{cat} from components final desulfation experiment.

peak assignments are listed in Table 4. Even though all of the components store NO_x, it is clear that MA has the least potential as a NO_x storage media. Sulfur spectra taken after sulfating for 1 h and after heating to 450 °C in 5% H_2O are shown in Fig. 8. Again, all of the components store sulfur, but the stability of sulfur species varies as seen in micro-reactor experiments. DRIFTS experiments will be discussed further in Section 4.

4. Discussion

A primary goal of this study is to highlight the individual behavior of components in a complex commercial LNT catalyst; however,

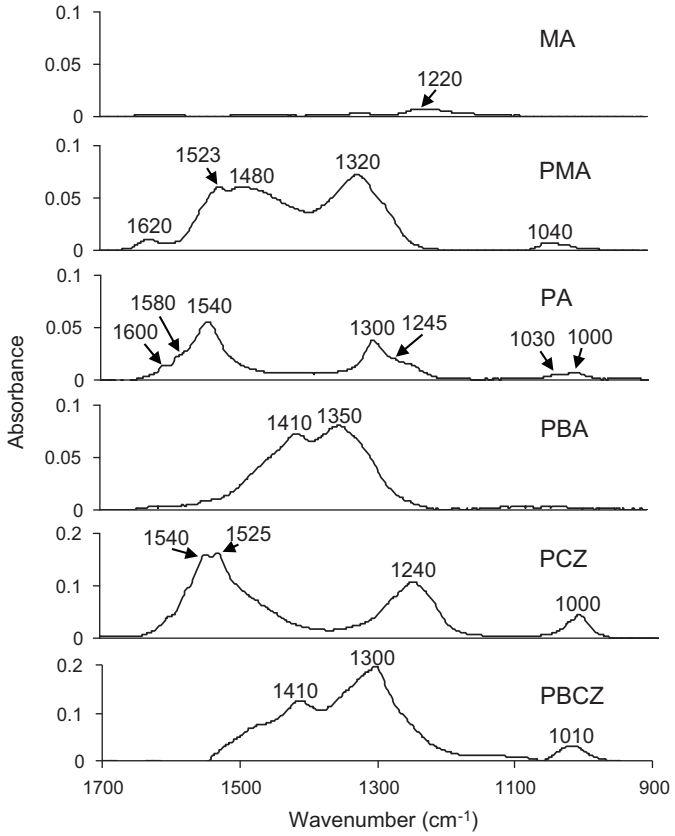

Fig. 7. DRIFTS spectra after 30 min of NO_x storage at 200 °C (300 ppm NO, 10% O_2, 5% H_2O, Ar balance). Spectra referenced to catalyst at $t = 0$. Different y-axes are used to enhance peak resolution.

a certain level of combining phases must be done to see the impact of the components. Therefore, the comparing and contrasting of a series of multi-phase catalysts was employed to highlight the roles of the components. As mentioned above, the commercial catalyst whose components were the focus of this study differs from the commonly studied model LNTs in several ways. The three primary differences are the use of ceria–zirconia as the storage phase support, the near absence of PGM on some phases of the washcoat, and the high level of $MgAl_2O_4$ employed in the washcoat. How these differences impact sulfate formation and stability are individually discussed below.

4.1. Ceria–zirconia support compared to γ-alumina

The supporting of the storage phase on ceria–zirconia rather than γ-alumina manifests itself in several ways that have already been reported, i.e. ceria improves low temperature LNT performance [33], increases WGS (water–gas shift) reactivity [37,38], and results in oxygen storage as the ceria moves to a higher oxidation state (Ce^{4+} in CeO_2) in the presence of oxygen compared to under rich conditions (Ce^{3+} in Ce_2O_3). Additionally, in physical mixtures of $Pt/Ba/Al_2O_3$ and Pt/ceria, the ceria phase has been shown to adsorb and release sulfur in a distinct region at lower temperatures than Ba-based sulfur [33]. The results shown in this study add to this list of effects with respect to sulfur uptake, the location and stability of the sulfur, and the desulfation behavior.

Starting with PA and PCZ, it is possible to compare how the supports both store and release sulfur. Fig. 2 shows the storage of sulfur for these supports is significantly different, as PA has sulfur breakthrough beginning after 1500 s and only stores 187 μmol/g_{cat} (Table 2), whereas there is essentially no breakthrough using PCZ

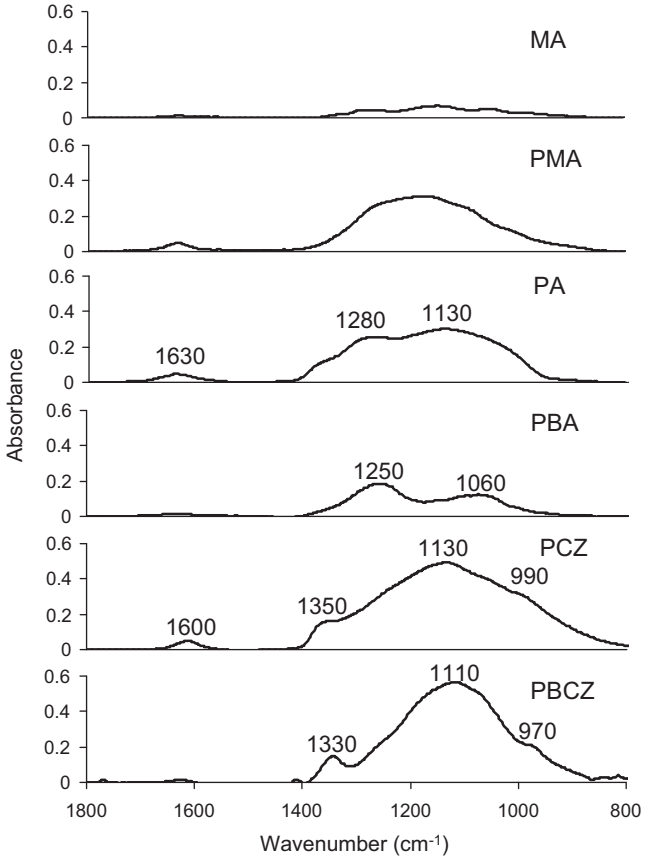

Fig. 8. DRIFTS spectra after 1 h of SO_2 storage at 200 °C. Conditions specified in Table 3, and spectra referenced to catalyst at $t = 0$.

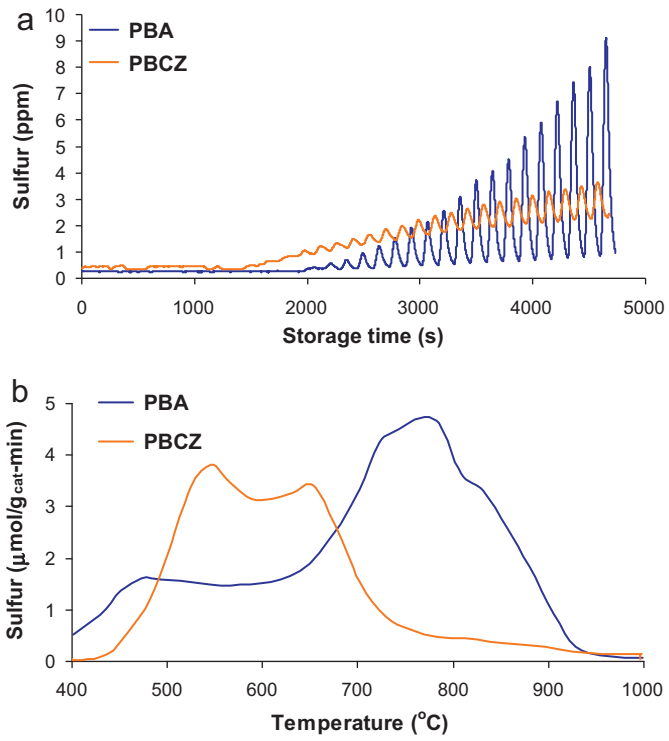

Fig. 9. Direct comparison of PBA and PBCZ (a) sulfation and (b) desulfation.

which stores 204 µmol/g_{cat} or essentially all of the sulfur fed to the reactor. When moving to the desulfation comparison in Fig. 5, the stability of the sulfates is shown to be considerably different as well. PA has a profile that is very broad and indicative of the heterogeneous nature of the γ-alumina support. Some of the sulfates are being removed at the temperature of sulfation (400 °C), 20% of the sulfates are removed before 464 °C (T_{20}), and they continue to be removed at high temperatures with 90% removed by 707 °C (T_{90}). PCZ on the other hand has a narrower desulfation profile. The initial release occurs at a moderately higher temperature, T_{20} = 494 °C, but the sulfates are completely removed at much lower temperatures, T_{90} = 570 °C. The T_{20} and T_{90} are listed for each component in Table 2. Interestingly, in the sulfated DRIFTS spectra in Fig. 8, both PA and PCZ show relatively similar peak locations. The primary difference is the more pronounced peak at 1280 cm^{-1} on PA during the initial sulfation at 200 °C.

From a LNT durability standpoint it is more desirable to have sulfur removal at temperatures that are as low as possible, but since it is expected that the majority of the sulfur will be on the Ba-based storage phase, it is most relevant to compare the sulfation and desulfation of PBA and PBCZ. Returning to the analyzed sulfur uptake listed in Table 2, it can be seen that PBA and PBCZ have similar uptake capacities for SO_2, 199 and 195 µmol/g_{cat}, respectively. However, an inspection of the effluent profiles (Fig. 2 and expanded in Fig. 9a) reveals that there are different dynamics occurring on these samples. There is a pronounced oscillation with PBA that is in sync with the lean to rich cycling that is a part of the sulfation step (Fig. 3). This oscillation is significantly muted in the PBCZ sample, illustrating that SO_2 is more likely to release from PBA in small quantities during the brief rich phase. Understanding this behavior helps explain how sulfur is stored on these samples in an axial profile. Choi et al. [7] have reported that the sulfur is dispersed in the commercial catalyst in a plug-like manner with respect to NO_x storage-reduction behavior, but the oxygen storage capacity (OSC) is impacted in a more gradual manner.

Combining our observations with these previous findings the schematic displayed in Fig. 10 is proposed to explain the behavior. Initially, for both samples the SO_2 is efficiently stored following a spillover mechanism near the Pt particles, such that the population of SO_2 on the Pt is low. As the surrounding oxides become sulfated, the transfer of SO_2 from the Pt to the oxide slows, and the population increases on the Pt surface. This is the state in the lean sulfation schematics in Fig. 10. The difference between PBA and PBCZ is that the ceria–zirconia phase in PBCZ contains oxygen that is available to form sulfates under rich conditions. Thus, when the conditions are switched from lean to rich the Pt-bound SO_2 can be captured on the ceria–zirconia phase of PBCZ, but immediately leaves PBA and cannot be readsorbed

How the catalyst sulfates is clearly important and helps explain how functionality is affected with increased sulfur loading. However, the most striking effect to employing a ceria zirconia support with Ba occurs in the desulfation profiles. Fig. 9b highlights this difference for the PBA and PBCZ samples where it can be seen that the desulfation profile is significantly shifted to lower temperatures. The T_{20} is 35 °C lower for PBCZ and T_{90} is 58 °C lower, but this quantification does not fully illustrate the impact. As seen in Fig. 5 and listed in Table 2, PCZ releases 90% of its sulfur by 570 °C. This generally correlates with the first desulfation peak for PBCZ, which has a peak release at 540 °C and suggests this initial peak is associated with sulfur on ceria–zirconia. The second peak in the PBCZ desulfation profile is centered near 650 °C, and must be associated with the Ba-phase due to the absence of any sulfur on PCZ above 600 °C. This peak is significantly lower than the peak release on PBA which is near 780 °C, and suggests a support effect that destabilizes the sulfates in the Ba-phase. The exact nature of this support effect is not clear, but it is expected to be akin to strong metal support interactions that have been a cornerstone of supported catalysis

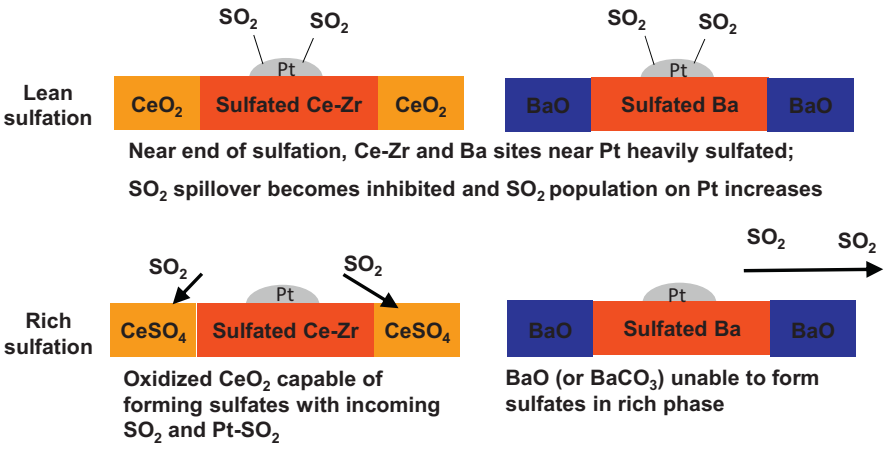

Fig. 10. Conceptual model of lean and rich sulfation dynamics on PBA and PBCZ.

research since the seminal work of Tauster et al. [39]; essentially this would be strong metal oxide–support interactions.

To study this support effect further, DRIFTS was applied to elucidate the state of the adsorbed species and if possible, identify which phases are associated with both sulfates and nitrates under typical exhaust conditions (Figs. 7 and 8). Fig. 8 shows the state of the catalyst after sulfating at 200 °C for each sample. Comparing PA to PBA, it can be observed that the initial sulfate formation is generally different, with PA having a more complex spectrum than the Ba-based PBA. Comparing PCZ to PBCZ in Fig. 8, it can be seen that the initial sulfation profiles are quite similar to each other, suggesting that the sulfur is adsorbing on both the ceria–zirconia support and the Ba storage component. In general, it is difficult to differentiate on which phase the sulfur is adsorbing due to the similarity in peaks for each material.

In contrast, the nitrate spectral features observed in Fig. 7 are significantly different for each component; therefore, to probe the location of the sulfates the catalysts were sulfated and NO_x was introduced to probe where nitrates were formed. These results are illustrated in Figs. 11–13 for PBA, PBZ and PBCZ, respectively. These figures each depict nitrate formation on the samples (a) before exposure to sulfur, (b) after heating in Ar/H_2O to 450 °C and stabilizing the sulfates, and (c) after attempting a mild desulfation at 500 °C

Table 4
Peak assignments (cm^{-1}) for adsorbed NO_x and SO_x species.

Component	Peak position (cm^{-1})	Adsorbed species
PA	1000, 1030, 1245, 1290, 1545, 1575, 1600	NO_3 on Al_2O_3
	1133, 1168, 1270, 1363	SO_3 on Al_2O_3
PCZ	1010, 1244, 1527, 1542	NO_3 on Ce
	1016, 1130, 1300, 1350	SO_3 on Ce
MA	1220	NO_x on $MgAl_2O$
	1050, 1140, 1270	SO_x on $MgAl_2O$
PMA	1020, 1280, 1545	NO_x on $MgAl_2O_4$
	1110, 1170	SO_x on $MgAl_2O$
PBA	1350, 1410	NO_3 on Ba
	1070, 1250	SO_3 on Ba
PBCZ	1200	NO_2 on Ba
	1300, 1350, 1410	NO_3 on Ba
	1300, 1410	NO_3 on Ce
	975, 1040, 1080, 1110, 1150, 1170, 1340, 1405	SO_3 on PBCZ

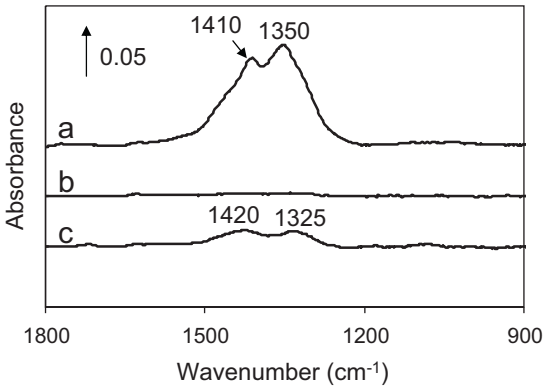

Fig. 11. DRIFTS spectra after 30 min of NO_x storage at 200 °C on PBA. (a) Nitrates formed before introduction of SO_2, referenced to $t = 0$ in step 3a in Fig. 1; (b) nitrates formed after sulfation and heating to 450 °C in 5% H_2O, referenced to $t = 0$ of step 3c; (c) nitrates formed after mildly desulfating to 500 °C in 5% H_2O and 0.79% H_2, spectra referenced to $t = 0$ of step 3d.

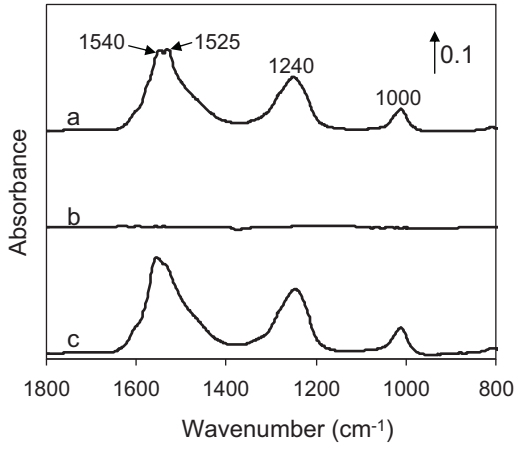

Fig. 12. DRIFTS spectra after 30 min of NO_x storage at 200 °C on PCZ. (a) Nitrates formed before introduction of SO_2, referenced to $t = 0$ in step 3a in Fig. 1; (b) spectra after SO_2 introduction and after heating to 450 °C in 5% H_2O, referenced to $t = 0$ of step 3c; (c) nitrates formed after mildly desulfating to 500 °C in 5% H_2O and 0.79% H_2, spectra referenced to $t = 0$ of step 3d.

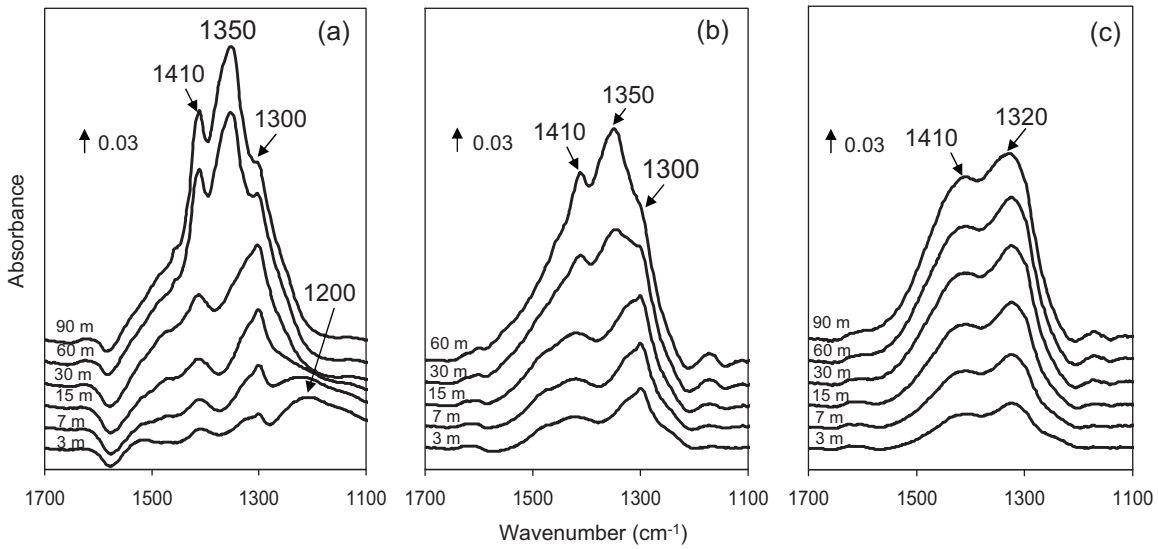

Fig. 13. DRIFT spectra during NO_x storage at 200 °C on PBCZ. (a) Nitrates formed before introduction of SO_2, referenced to $t = 0$ in step 3a in Fig. 1; (b) spectra after SO_2 introduction and after heating to 450 °C in 5% H_2O, referenced to $t = 0$ of step 3c; (c) nitrates formed after mildly desulfating to 500 °C in 5% H_2O and 0.79% H_2, spectra referenced to $t = 0$ of step 3d.

in H_2. Each spectra is referenced to $t = 0$ of the given nitrate adsorption sequence, such that the sulfate peaks will not be observed in the recorded spectra because they will be part of the background spectra. In Fig. 11, it can be seen that nitrates that readily form on PBA before the introduction of sulfur are completely blocked after 60 min of 30 ppm SO_2 (this sample size is very small, <1 mg, and thus it is not surprising that no nitrates are observed). Upon reducing the sample in H_2 a small portion of the storage sites are recovered (~20%), and nitrates can form again. In contrast, Fig. 12 shows that even though the PCZ sample loses all of its storage sites upon sulfating, that heating to 500 °C in H_2 allows the recovery of all of the storage capacity. However, this only illustrates the difference between ceria–zirconia and barium, therefore, PBCZ was also examined. Fig. 13 shows both the impact of sulfation and complex progression of nitrate formation on the sample. The fresh spectrum for PBCZ is significantly more complex than the PBA or PCZ samples. The initial nitrates observed are at ~1300 and 1400 cm^{-1} similar to what is observed on the PBA sample (although slightly offset). After 60 min, a peak at 1350 cm^{-1} grows in and begins to dominate the spectrum. It is difficult to identify this peak, as it does not overlap with the PCZ or the PBA peaks; however, a possibility is that it represents the bulk nitrate formation. After sulfating and desulfating to 500 °C in H_2, this peak at 1350 cm^{-1} does not reappear; in fact, nitrates are only observed at 1320 and 1410 cm^{-1}. These features very closely resemble the peaks on PBA, rather than PCZ, and illustrate that the storage sites that have been desulfated are in fact associated with Ba rather than the ceria–zirconia support. This peak is also on the order of the nitrates stored on the fresh sample (~70%). This further illustrates that the ceria zirconia is not simply a support, but in fact alters the behavior of the Ba-phase and changes the desulfation characteristics.

4.2. Comparison of phases with and without PGM

As noted earlier the MA phase in the commercial catalyst has little to no PGM. To illustrate the impact of PGM on the different components, MA and PMA are used, and to illustrate how the behavior changes when PGM is in the vicinity of a non-PGM phase, a physical mixture of PA + MA is employed. First looking at the sulfation behavior in Fig. 2, sulfur breakthrough begins after only 250 s on the MA sample and quickly begins to approach the inlet concentration of 30 ppm. The addition of Pt to the MA component (PMA) dramatically increases the sulfur storage capacity from 112 to 193 $\mu mol/g_{cat}$. This highlights that the oxidation of SO_2 to SO_3 is an important step in the formation of sulfates, analogous to NO to NO_2 oxidation in nitrate storage. However, when employing a physical mixture of PA and MA, much like what is found in the commercial catalyst, the overall sulfation behavior is more like PMA or PA, than MA. It could be argued that the sulfur is simply going to the PA portion of the physical mixture, however, the breakthrough time occurs later in PA + MA compared to PA, even though the PA portion is halved (it should be noted that the same total sample mass was used for each experiment, i.e. for a 75 mg physical mixture, 37.5 mg of each component was used). These results suggest that the proximity of the PGM to the storage phase is not inherently critical for capture, particularly for sulfates; therefore, it is possible that the MA phase could behave as a sulfur and nitrate adsorption medium in the commercial catalyst even though there is not significant PGM on the MA phase.

The desulfation profiles of these samples also corroborate this claim (Fig. 14). MA has a very high release profile for sulfate with a T_{20} of 653 °C and a T_{90} of 816 °C. The addition of Pt to MA (PMA), results in a broad release profile, with a much lower T_{20} of 544 °C and a T_{90} of 789 °C. As discussed earlier PA has low temperature release. The physical mixture PA + MA results in a desulfation profile that mimics both PA and PMA, but not MA. These results suggest that the proximity of PGM to sulfates is not critical for their release, which is quite surprising. It is not clear how the reductant is interacting with the non-PGM component, but there must be some release of an intermediate into the gas-phase that can readily adsorb on the MA-phase and release sulfates at temperatures lower than when MA is by itself.

4.3. Role of $MgAl_2O_4$ (MA) in commercial catalyst

One of the first goals of this study was to determine the role of the large amount of $MgAl_2O_4$ in the commercial catalyst. The results from the previous section suggest that it may be useful as a sulfur trap that can be regenerated without direct contact with PGM. To ensure that a fair comparison could be made for the individual components, a physical mixture of PBCZ + MA was used to simulate the commercial catalyst. Fig. 2 illustrates this sample is very effective

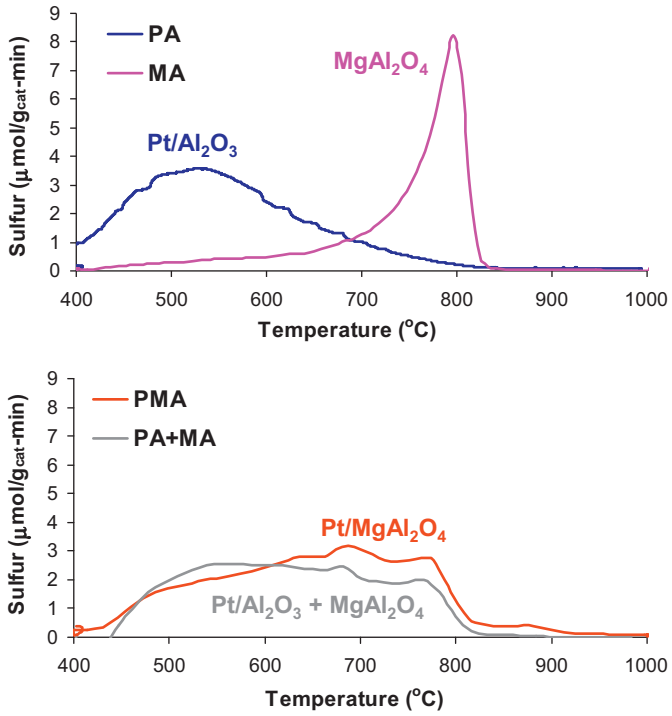

Fig. 14. Desulfation profiles of PA, MA, PMA and the physical mixture PA + MA.

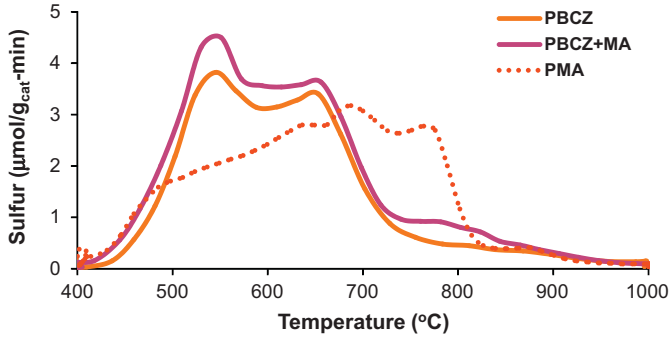

Fig. 15. Desulfation profiles of PBCZ, the physical mixture PBCZ + MA, and PMA.

in trapping SO_2 as there was no sulfur breaking through during the procedure. In comparing this to PBCZ this is quite remarkable as more sulfur is captured in the PBCZ + MA physical mixture even though half of the PBCZ was employed. However, investigation of the sulfur release profiles (highlighted in Fig. 15) does not show a dramatic shift in the desulfation temperature. There is consistently more sulfur being released from the PBCZ + MA sample with perhaps a slight increase at the highest temperatures, and even though the differences are not dramatic, they are significant and suggest this is one of the roles of MA in the commercial sample.

5. Summary and conclusions

Components found in a commercial lean NO_x trap were studied in order to determine their impact on sulfate storage and release. Through studying the modes of sulfate formation and desulfation on the individual components and physical mixtures the chemical behavior in the presence of sulfur was determined. The key findings are summarized below:

- Supporting barium on ceria–zirconia rather than alumina dramatically decreases the sulfate stability.
- The oxygen storage behavior of the ceria–zirconia plays a role in the storage of sulfur during cycling conditions.
- Close proximity of Pt to the sulfate storage medium is not essential to either sulfate formation or desulfation.
- $MgAl_2O_4$ without Pt can play a role as a sulfur storage medium in physical mixture of catalysts, such as the case in a commercial washcoat.

Additionally, the identification of nitrate and sulfate IR adsorption bands for each component is outlined. Of these findings, the impact of ceria on desulfation temperature has the most implications on the future of LNT research. It is clear that the support dramatically impacts barium sulfate stability. Investigations that can understand this metal oxide/support interaction will greatly advance the science and could lead to the next generation of LNTs, especially if a support is predicted/identified that can decrease sulfate stability without also storing oxygen.

Acknowledgments

Research sponsored by the U.S. Department of Energy, Office of Energy Efficiency and Renewable Energy, Vehicle Technologies Program, under contract DE-AC05-00OR22725 with UT-Battelle, LLC.

References

[1] W.S. Epling, L.E. Campbell, A. Yezerets, N.W. Currier, J.E. Parks, Catal. Rev. 46 (2004) 163.
[2] S. Roy, A. Baiker, Chem. Rev. 109 (2009) 4054.
[3] W.S. Epling, G.C. Campbell, J.E. Parks, Catal. Lett. 90 (2003) 45.
[4] L. Xu, G. Graham, R. McCabe, Catal. Lett. 115 (2007) 108.
[5] J.S. Choi, W.P. Partridge, J.A. Pihl, C.S. Daw, Catal. Today 136 (2008) 173.
[6] J.S. Choi, W.P. Partridge, C.S. Daw, Appl. Catal. B 77 (2007) 145.
[7] J.S. Choi, W.P. Partridge, M.J. Lance, L.R. Walker, J.A. Pihl, T.J. Toops, C.E.A. Finney, C.S. Daw, Catal. Today 151 (3-4) (2009) 354.
[8] J.-S. Choi, W.P. Partridge, M.J. Lance, L.R. Walker, J.A. Pihl, T.J. Toops, C.E.A. Finney, C.S. Daw, Catal. Today 151 (2010) 354.
[9] J.-S. Choi, W.P. Partridge, N.A. Ottinger, J.A. Pihl, T.J. Toops, M.J. Lance, C.E.A. Finney, C.S. Daw, 12th CLEERS Workshop, Dearborn, MI, 2009, http://www.cleers.org/workshops/workshop12/index.php.
[10] F. Rohr, S.D. Peter, E. Lox, M. Kogel, A. Sassi, L. Juste, C. Rigaudeau, G. Belot, P. Gelin, M. Primet, Appl. Catal. B 56 (2005) 201.
[11] L. Limousy, H. Mahzoul, J.F. Brilhac, P. Gilot, F. Garin, G. Maire, Appl. Catal. B 42 (2003) 237.
[12] L. Limousy, H. Mahzoul, J.F. Brilhac, F. Garin, G. Maire, P. Gilot, Appl. Catal. B 45 (2003) 169.
[13] Z. Liu, J.A. Anderson, J. Catal. 228 (2004) 243.
[14] H. Mahzoul, L. Limousy, J.F. Brilhac, P. Gilot, J. Anal. Appl. Pyrol. 56 (2000) 179.
[15] T.J. Toops, Y. Ji, V. Easterling, M. Crocker, J. Theis, J. Ura, R.W. McCabe, 10th CLEERS Workshop, May 1–3, 2007, www.cleers.org.
[16] J.H. Kwak, D.H. Kim, J. Szanyi, C.H.F. Peden, Appl. Catal. B 84 (2008) 545–551.
[17] S. Elbouazzaoui, E.C. Corbos, X. Courtois, P. Marecot, D. Duprez, Appl. Catal. B 61 (2005) 236.
[18] D.H. Kim, J.H. Kwak, X. Wang, J. Szanyi, C.H.F. Peden, Catal. Today 136 (2008) 183.
[19] L. Kylhammar, P. Carlsson, H.H. Ingelsten, H. Gronbeck, M. Skoglundh, Appl. Catal. B 84 (2008) 268.
[20] G. Corro, A. Velasco, R. Montiel, Catal. Commun. 2 (2001) 369.
[21] S.W. Nam, G.R. Gavalas, Appl. Catal. 55 (1989) 193.
[22] M. Waqif, J. Bachelier, O. Saur, J.C. Lavalley, J. Mol. Catal. 72 (1992) 127.
[23] E. Xue, K. Seshan, J.R.H. Ross, Appl. Catal. B 11 (1996) 65.
[24] H.C. Yao, H.K. Stepien, H.S. Gandhi, J. Catal. 67 (1981) 231.
[25] M. Bensitel, M. Waqif, O. Saur, J.C. Lavalley, J. Phys. Chem. 93 (1989) 6581.
[26] W.P. Cheng, J.G. Yang, M.Y. He, Catal. Commun. 10 (2009) 784.
[27] J.A. Wang, L.F. Chen, R. Limas-Ballesteros, A. Montoya, J.M. Dominguez, J. Mol. Catal. A 194 (2003) 181.
[28] J. Wang, C. Li, Appl. Surf. Sci. 161 (2000) 406.
[29] M. Waqif, O. Saur, J.C. Lavalley, Appl. Catal. 71 (1991) 319.
[30] G. Fornasari, R. Glockler, M. Livi, A. Vaccari, Appl. Clay Sci. 29 (2005) 258.
[31] J. Twu, C.J. Chuang, K.I. Chang, C.H. Yang, K.H. Chen, Appl. Catal. B 12 (1997) 309.
[32] P. Bazin, O. Saur, J.C. Lavalley, G. Blanchard, V. Visciglio, O. Touret, Appl. Catal. B 13 (1997) 265.
[33] Y. Ji, T.J. Toops, M. Crocker, Catal. Lett. 119 (2007) 257.

[34] T.J. Toops, B.G. Bunting, K. Nguyen, A. Gopinath, Catal. Today 123 (2007) 285.
[35] D. McLaughlin, F. Meunier, J.P. Breen, R. Burch, 3rd International Taylor Conference, Belfast, N., Ireland, 2004.
[36] T.J. Toops, D.B. Smith, W.S. Epling, J.E. Parks, W.P. Partridge, Appl. Catal. B: Environ. 58 (2005) 255.
[37] G. Jacobs, L. Williams, U. Graham, D.E. Sparks, B.H. Davis, Appl. Catal. A 252 (2003) 107.
[38] A.A. Phatak, N. Koryabkina, S. Rai, J.L. Ratts, W. Ruettinger, R.J. Farrauto, G.E. Blau, W.N. Delgass, F.H. Ribeiro, Catal. Today 123 (2007) 224.
[39] S.J. Tauster, S.C. Fung, R.L. Garten, J. Am. Chem. Soc. 100 (1) (1978) 170.